Temperature-dependent structure, elasticity, and entropic stability of Bi phases on Cu{111}

R. van Gastel,[1] D. Kaminski,[2,3] E. Vlieg,[2] and B. Poelsema[1]

[1]*Physics of Interfaces and Nanomaterials, MESA+ Institute for Nanotechnology, University of Twente, P.O. Box 217, 7500 AE Enschede, The Netherlands*

[2]*Radboud University Nijmegen, Institute for Molecules and Materials, Heyendaalseweg 135, 6525 AJ Nijmegen, The Netherlands*

[3]*Department of Chemistry, University of Life Sciences in Lublin, Akademicka 13, 20-950 Lublin, Poland*

(Received 7 October 2013; published 25 February 2014)

We have used low energy electron microscopy (LEEM) to characterize the structure and stability of Bi phases on Cu{111}. As a function of temperature we find that the Cu{111}($\sqrt{3} \times \sqrt{3}$)R30°-Bi surface alloy phase gradually dealloys and is fully depleted from Bi at a temperature of 803 K. The dealloying leads to a defect induced change of its elastic properties. The Bi surface alloy phase coexists with a Bi overlayer phase that exhibits a sharp decrease in density in a narrow temperature interval just below the temperature where the surface alloy phase has fully dealloyed. LEEM is used to directly evaluate the structure as well as the entropic contributions that determine the stability of each of the phases.

DOI: 10.1103/PhysRevB.89.075431 PACS number(s): 81.16.Dn, 68.37.Nq, 68.47.De, 68.35.Md

I. INTRODUCTION

Surface confined mixing of two elements that are bulk immiscible allows for a tailoring of the physical properties of a surface active region [1–4]. As a result of the low-dimensional character of thin films many properties arise that have no analog in the bulk. A common observation in these systems however is that the properties of the various intermetallic phases that form are strongly temperature dependent. Because of the large number of particles that are involved, first-principles methods generally have only limited ability to accurately predict the entropic contributions that are at the origin of the temperature-dependent properties. Moreover, experiments that yield a comprehensive picture of all relevant parameters are difficult to perform with a single technique [5]. Diffraction experiments typically allow for an accurate characterization of the atomic structure, but average out the spatial diversity of the various phases that coexist [6]. High resolution forms of microscopy with a narrow field of view allow for a detailed characterization of atomic composition and kinetics, but fail to dynamically visualize the thermodynamically driven collective behavior that determines the stability of different surface phases on a larger length scale. In this paper we detail low energy electron microscopy (LEEM) measurements that were used to obtain a comprehensive picture of the structure and stability of Bi phases on Cu{111}. The present results complement previous publications that detailed the atomic relaxation of Bi and an order-disorder transition in a Bi/Cu{111} surface alloy phase [7], as well as the kinetics of formation of that phase [8].

II. Bi/Cu{111} AND EXPERIMENTAL DETAILS

When Bi is deposited on Cu{111} it initially forms a random surface alloy, which we refer to as the (1×1) phase [8]. Upon reaching a Bi coverage of 1/3 ML (expressed in Cu unit cells), the surface alloy assumes an ordered ($\sqrt{3} \times \sqrt{3}$)R30° substitutional alloy structure. Any additional Bi that is deposited in excess of 1/3 ML is incorporated in an overlayer phase [6,9–11]. The precise structure of the overlayer phase depends on coverage and temperature and has been described in detail elsewhere [12]. In what follows we will refer to the Cu{111}($\sqrt{3} \times \sqrt{3}$)R30°-Bi surface alloy phase simply as the $\sqrt{3}$ phase or surface alloy phase. The overlayer and $\sqrt{3}$ phase self-assemble into periodic domain structures. The real-time, large field of view imaging capabilities of low energy electron microscopy [13] were used to monitor the evolution of the two Bi phases and characterize their properties in both real and reciprocal space. For our experiments a Cu single crystal was mechanically polished and aligned to the {111} crystallographic direction with an accuracy better than 0.1°. The Cu{111} surface was further prepared by repeated cycles of Ar^+ ion sputtering and annealing until LEEM images revealed large defect-free terraces. Bi was vapor deposited from a Knudsen cell. An accurate temperature measurement was achieved by comparing to previous SXRD and LEEM data sets that we have for this system and cross correlating the observed phase transitions and other phenomena [6,12].

III. TEMPERATURE-DEPENDENT Bi COVERAGE OF THE $\sqrt{3}$ ALLOY

Bi was deposited to a total coverage of 0.376 ML and bright-field LEEM images were recorded to monitor the area fractions of the $\sqrt{3}$ and overlayer phases as a function of temperature. A sequence of images that illustrates our observations above 700 K is shown in Fig. 1. For the behavior of both phases below 700 K, and images thereof, we refer the reader to Ref. [7]. Initially the $\sqrt{3}$ (dark) and overlayer (bright) phases coexist, each occupying approximately half of the visible surface area. With increasing temperature the relative area fraction occupied by the overlayer phase increases. At a temperature of 803 K the dealloying of the $\sqrt{3}$ phase is complete and the overlayer phase occupies the entire field of view, as is visible in Fig. 1(c). After this initial dealloying of the $\sqrt{3}$ phase, the temperature of the substrate was ramped up and down through 803 K three more times. The temperature of the sample was held constant for several minutes at 803 K after each cycle. During this period no changes in reflected intensity were observed, indicating that the rate of desorption of Bi is small on that time scale. However, after each cycle, i.e., change in temperature, the electron reflectivity of the

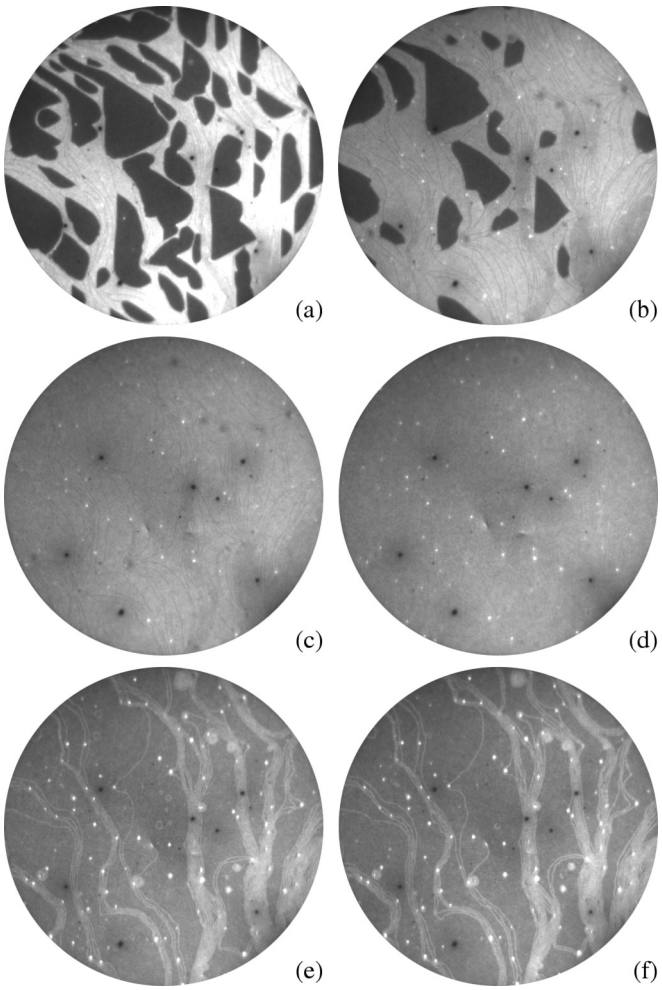

FIG. 1. 10 μm field of view (FOV) LEEM images recorded at 21.9 eV electron energy and a total Bi coverage of 0.376 ML. (a) $T = 776$ K. The $\sqrt{3}$ (dark) and overlayer (bright) phases coexist, each occupying approximately half of the visible area. (b) $T = 801$ K. Upon increasing temperature the area fraction of the $\sqrt{3}$ phase is reduced. (c) $T = 803$ K. Upon reaching 803 K the $\sqrt{3}$ phase dealloys and a diluted overlayer phase occupies the entire visible area. (d)–(f) $T = 803$ K. Subsequent images recorded after further thermal cycling through the dealloying temperature yield a reduced density of the overlayer phase at 803 K, as well as the formation of three-dimensional structures, visible as bright spots. Dark spots that are visible in all images are defects in the microchannel plate detector unit.

overlayer phase at 803 K was reduced and an increasing number of three-dimensional structures could be observed in the LEEM images, visible as bright spots in Figs. 1(d)–1(f). The 3D structures typically form upon realloying when the substrate is cooled back down through 803 K. This indicates that Cu adatoms that are made available when the $\sqrt{3}$ alloy reforms, make a three-dimensional, but finite sized Bi-Cu alloy. Neither the stoichiometry of the alloy, nor the precise shape or distribution of the two elements, can be probed with LEEM. This 3D alloy structure apparently has a lower free energy at 803 K than either of the two surface phases. It leads to a reduction of the amount of Bi that is available elsewhere on the surface to form the overlayer and $\sqrt{3}$ phases after cooling.

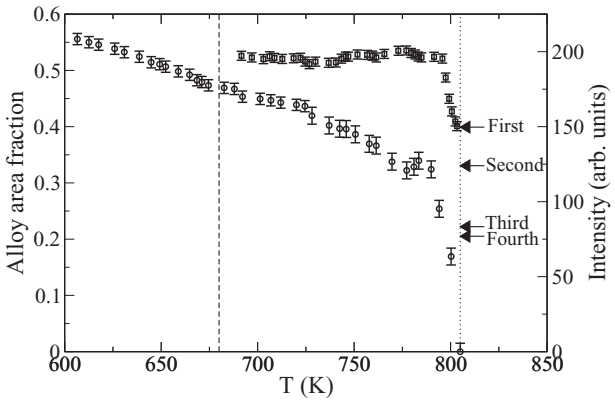

FIG. 2. Relative area fraction occupied by the $\sqrt{3}$ phase (circles) versus temperature for a total Bi coverage of 0.376 ML. The dashed line marks the temperature where changes in the domain patterns occur as a result of an order-disorder transition in the $\sqrt{3}$ phase. The dotted line marks the dealloying temperature. Data acquired at temperatures greater than 725 K are subject to a larger uncertainty because of a higher heating rate and associated thermal drift of the images. The electron reflectivity of the overlayer phase (squares) is also plotted versus temperature. It remains constant up to a temperature of 796 K, after which it drops sharply. The reflectivity of the overlayer phase after each temperature cycle is indicated by the arrows in the right hand side of the figure.

The same 3D alloy structure can be observed to form during growth at lower temperatures, see, e.g., Fig. 1(d) of Ref. [8].

In Fig. 2 the area fraction A of the $\sqrt{3}$ phase is plotted versus temperature for the first temperature cycle. For a constant total Bi coverage the relative fraction of the sample that is covered by the $\sqrt{3}$ phase decreases as a function of temperature. Knowing the total Bi coverage θ_{Bi}, the Bi coverage per Cu unit cell of each of the two phases can be calculated using the lever rule

$$\theta_{\mathrm{Bi}} = A\theta_{\sqrt{3}} + (1 - A)\theta_{\mathrm{overlayer}}. \quad (1)$$

The temperature-dependent coverage of the $\sqrt{3}$ phase can in principle be directly determined from the area fraction it occupies at a coverage of 0.376 ML. The overlayer fulfills the role of a reservoir that accommodates Bi that is expelled from the $\sqrt{3}$ phase. Some of the Bi may however already reside in 3D structures and therefore a first complication in this procedure is that a calibration point is needed to determine the absolute coverage of the $\sqrt{3}$ phase. This calibration point is provided by the order-disorder transition that was measured previously [7]. The signature changes that take place in the domain patterns, as a result of this transition, occur at 680 K. We therefore set the coverage of the $\sqrt{3}$ phase equal to the hard-hexagon critical coverage of 0.276 ML at 680 K. A second complication in determining the Bi coverage of the $\sqrt{3}$ phase is posed by the potentially temperature-dependent Bi coverage of the overlayer phase. Plotted on the right-hand side of Fig. 2 is the electron reflectivity of the overlayer phase as a function of temperature. At temperatures exceeding 480 K, the overlayer phase is in a disordered, liquid state [12]. The electron reflectivity of a randomly distributed phase of particles was demonstrated to provide an estimate of the density of that

phase [14–16]. From the data plotted in Fig. 2, we conclude that the electron reflectivity is not only a sensitive measure for the density of a dense Bi overlayer phase, but that the density of the overlayer phase is approximately constant until 796 K. To reconcile the total amount of Bi that is deposited with the relative fractions of the two visible phases, and produce a coverage of the $\sqrt{3}$ phase of 0.276 ML at 680 K, the Bi coverage of the overlayer phase was used as a free parameter. The value that yields best agreement is a Bi coverage of the overlayer of 0.465 ± 0.003 ML [8] for the temperature interval from 600 to 796 K. This value is consistent with the coverage of the crystalline overlayer phase of 0.5 ML that was determined for a crystalline overlayer phase at room temperature using surface x-ray diffraction (SXRD) [6,12].

Above 796 K the LEEM images of Figs. 1(a)–1(b) indicate that the Bi coverage of the overlayer phase decreases rapidly as the area fraction of the $\sqrt{3}$ phase decreases to zero. This change in density of the overlayer phase is unexpected. Naively one would expect the alloy phase to gradually dealloy until it is fully depleted. The Bi that is released from the alloy would be incorporated in the overlayer, leading to small, but measurable changes in the area fractions of both phases. Eventually the overlayer would remain and coexist with the bare Cu(111) substrate. Instead what occurs is that the density of the overlayer decreases substantially. In Sec. V we discuss the physical origin of this density change in more detail. Since the measured electron reflectivity decreases linearly with temperature above 796 K, we use a Bi density that decreases linearly from 0.465 to 0.376 ML from 796 to 803 K to establish the Bi coverage of the $\sqrt{3}$ phase. The resulting Bi coverage of the $\sqrt{3}$ phase that this analysis yields for the entire temperature range is shown in Fig. 3. The data are plotted concurrently with the previously measured relaxation data for Bi in the $\sqrt{3}$ alloy phase [7]. The data yield a tendency

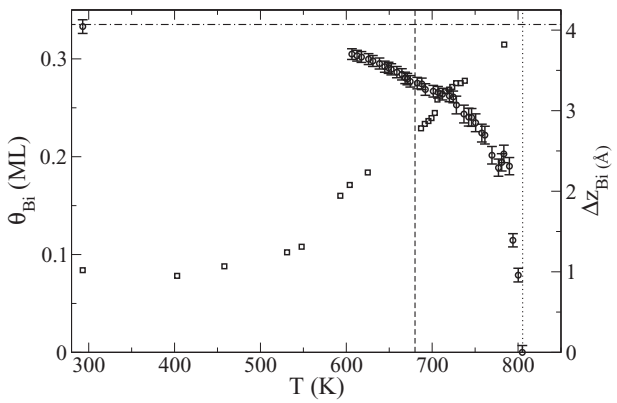

FIG. 3. Temperature-dependent Bi coverage of the $\sqrt{3}$ phase (circles) as derived from the area fractions and reflectivity data shown in Fig. 2. The absolute Bi coverage decreases with temperature. It passes through the hard-hexagon critical coverage of 0.276 ML at 680 K (dashed line) and becomes equal to zero at the dealloying temperature of 803 K (dotted line). For completeness the outward relaxation of the Bi atoms (squares) is also plotted to fully characterize the temperature-dependent structure of the $\sqrt{3}$ phase. The outward relaxation at which dealloying takes place is marked by the dashed-dotted line. The same line also denotes the 0.333 ML low temperature coverage limit of the $\sqrt{3}$ phase.

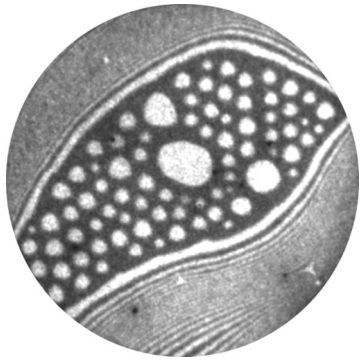

FIG. 4. 2 μm FOV LEEM image of a droplet pattern of the Bi overlayer phase (bright) created in the matrix of a $\sqrt{3}$ alloy phase (dark). The image was recorded at an electron energy of 20.4 eV, at a temperature of 639 K and was used to perform the trajectory analysis that yielded the data of Fig. 5.

for lower Bi densities and larger outward relaxations with increasing temperature, indicating that the energetic gains that drive the formation of the alloy phase are reduced as a function of temperature [17]. When the data of Fig. 3 are combined with the electron reflectivity and SXRD data of the overlayer phase [6], a complete and comprehensive picture of the temperature-dependent structure of the $\sqrt{3}$ phase is realized.

IV. ELASTIC PROPERTIES OF THE $\sqrt{3}$ PHASE

Having established the details of the temperature-dependent atomic structure of the $\sqrt{3}$ alloy, we now address the elastic properties of that phase. The $\sqrt{3}$ alloy forms a self-assembled domain pattern with the overlayer phase, an example of which is shown in Fig. 4. This indicates that a significant mismatch in surface stress exists between the two phases. The gain in elastic energy that results from relaxations at the boundaries of the domains acts as a stabilizing force for the two-dimensional domain patterns. To measure the difference in the stress tensor of the two phases we have followed the same approach that was previously used to gauge the stress mismatch between similar phases in the Pb/Cu{111} system [18]. The strength of the interactions was analyzed by measuring the thermal motion in a dense 2D droplet configuration, shown in Fig. 4. Because of the significant order in these arrays, each 2D droplet fluctuates around its "equilibrium" position. The size of the fluctuations is determined by the strength of the interactions between 2D droplets. The interaction energy between two circular stress domains decays as the inverse cube of their separation [19],

$$U(r_{ij}) = g\frac{A_i A_j}{r_{ij}^3}, \tag{2}$$

where A_i is the area of 2D droplet i and r_{ij} is the distance between 2D droplets i and j. Assuming an isotropic elastic substrate [18,20], the interaction strength g is defined by

$$g = \frac{(\Delta\sigma)^2(1-\nu^2)}{\pi E}, \tag{3}$$

where $\Delta\sigma$ is the difference in surface stress between the $\sqrt{3}$ and the overlayer phase, and E and ν are the Young's modulus and Poisson's ratio of the substrate, respectively. The interaction strength g follows directly from the magnitude of the thermal fluctuations of the center of mass of the droplets. The position of individual droplets is analyzed in the context of the position of surrounding droplets. While taking care to avoid edge effects, the surrounding droplets define an equilibrium position for a droplet that typically deviates from its actual position. The difference is a measure for the magnitude of the thermal excitation. The analysis was performed for five different temperatures below 680 K, where the feature size of the domain pattern is small enough to allow for such an analysis. To estimate g from the data, instead of plotting distributions of the spatial deviation, we plot distributions of the thermal excitation energy $\Delta U/g$, defined as the calculated energy of the 2D droplet minus the equilibrium energy. Figure 5(a) shows the measured excitation for the 2D droplet configuration of Fig. 4. The distributions are consistent with the exponential Boltzmann statistics one expects from thermal fluctuations, i.e., the probability of ΔU is proportional to $\exp(-\Delta U/kT)$. Contrary to the case of Pb/Cu{111}, however, the data does not collapse onto one single curve and a temperature dependence of the stress mismatch can be discerned. Figure 5(b) shows the values of $\Delta\sigma$ that were obtained by fitting the distribution to $\exp(-\Delta U/kT)$, and using Eq. (3) to obtain $\Delta\sigma$, with values of 130 GPa and 0.34 for E and ν [21].

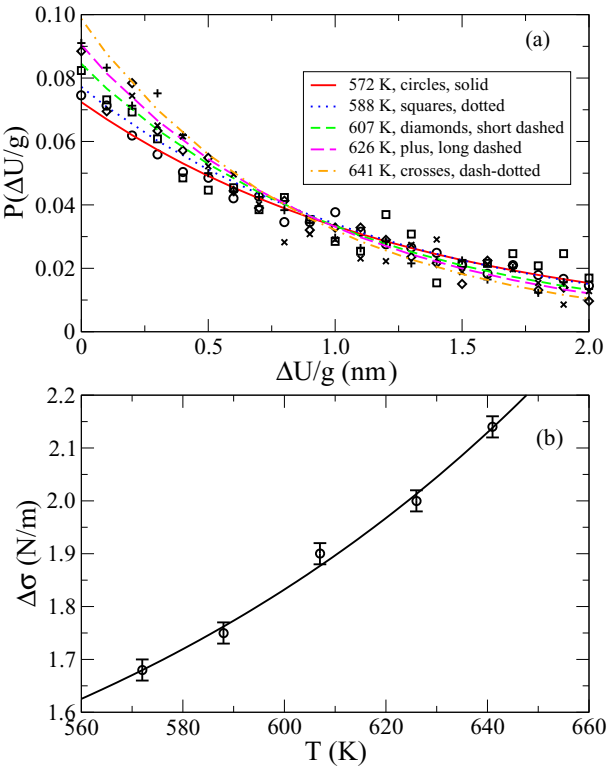

FIG. 5. (Color online) (a) Probability distribution for center of mass displacements of Bi overlayer islands measured for five different temperatures for approximately 50 islands over 2000 images for each temperature. The distributions are fitted with exponential curves. (b) Stress mismatch as a function of temperature as derived from the Boltzmann distributions of (a). The fit to the data was made using the assumption of a linearly changing stress mismatch with defect density and error bars represent the standard error that is obtained from a least squares fit of (a).

To interpret the changing value of $\Delta\sigma$ for the temperature range from 572 to 641 K, we note that it is the difference of the normal, in-plane components of the stress tensor of the $\sqrt{3}$ phase and the 2D liquid overlayer phase:

$$\Delta\sigma = \sigma_{\sqrt{3}} - \sigma_{\text{2D-liq}}. \tag{4}$$

The stress tensor characterizes the elastic response of both phases to an externally applied force. In the situation described here, strain caused by a stress mismatch at the interface of the two phases is mediated by a strain field in the substrate. The nature of the two phases is however fundamentally different. The $\sqrt{3}$ phase can be characterized as an ordered crystalline solid [7]. It is a commensurate phase that has to remain in registry with the substrate. The overlayer phase is in a fully incommensurate, liquid state and has freedom to expand or contract [12]. As a consequence, the magnitude of the elastic response of both phases is anticipated to be of a different order of magnitude. Similar differences are observed for bulk phases when comparing the bulk moduli of solids and liquids [22]. The bulk modulus characterizes the compressibility of matter and is typically between one and two orders of magnitude smaller for a liquid than for a solid. We therefore assume that $\sigma_{\sqrt{3}} \gg \sigma_{\text{2D-liq}}$ and $\Delta\sigma = \sigma_{\sqrt{3}}$. This assumption allows us to directly interpret the change in $\Delta\sigma$ in terms of temperature-dependent changes in the structure of the $\sqrt{3}$ phase.

We have previously demonstrated that the stress mismatch between the $\sqrt{3}$ phase and the overlayer phase is strongly affected by the degree of long-range order of the $\sqrt{3}$ phase [7]. This observation indicates that it is not so much the varying Bi density that alters the elastic response of the $\sqrt{3}$ phase, but rather the varying occupation of each of the three possible sublattices. The Bi coverage of the three sublattices of the $\sqrt{3}$ phase, as calculated using the hard-hexagon model [23], is plotted in Fig. 6. The Bi coverage in the two minority sublattices represents the defect density of the $\sqrt{3}$ structure. It

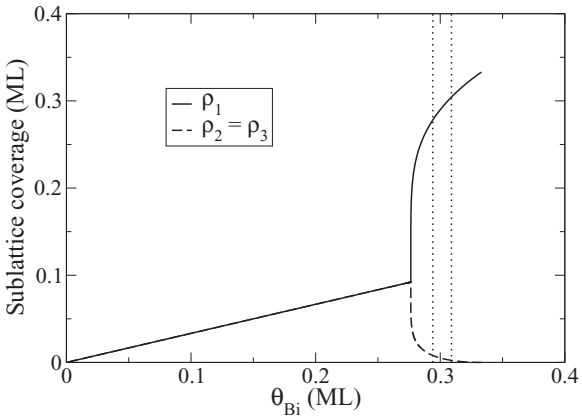

FIG. 6. Bi coverage of the three sublattices of the $\sqrt{3}$ phase calculated using the hard-hexagon model. The coverage of the minority sublattices 2 and 3 is indicated by a dashed line. The dotted vertical lines define the coverage range from 572 to 641 K that was probed in Fig. 5.

increases gradually, but significantly, in the coverage range that corresponds to the temperature interval for which the stress mismatch was measured and is indicated by dotted lines in Fig. 6. In the regime where the defect density is still sufficiently dilute, the surface Lamé constants that define the stress tensor are modified by the defect density in a linear fashion [24]. For an isotropic surface

$$\lambda(T) = \lambda_0 + 2\Lambda\rho_2(T),$$
$$\mu(T) = \mu_0 + 2M\rho_2(T), \tag{5}$$

where the magnitude of Λ and M is defined by the details of the elastic response of off-site Bi defects. The stress tensor is defined as

$$\sigma_{\sqrt{3}}(T) = \lambda(T) + 2\mu(T)$$
$$= \lambda_0 + 2\mu_0 + 2(\Lambda + 2M)\rho_2(T). \tag{6}$$

Because we have already characterized the defect density, an opportunity exists to experimentally verify the validity of defect-induced hardening of a two-dimensional system. The solid line in Fig. 5 was fitted to the data using Eq. (6). It describes the experimental data remarkably well, and further confirms the role that off-site Bi defects play in determining the elastic properties of the $\sqrt{3}$ phase.

V. ENTROPIC STABILITY

SXRD measurements have previously demonstrated how the overlayer phase changes from an ordered, solid phase, to an orthorhombically ordered liquid, to a disordered liquid with increasing temperature [12]. For all temperatures that were used in the experiments reported here, the overlayer is in a disordered liquid state. At a temperature of 796 K, however, the reflected intensity of the overlayer phase that is plotted in Fig. 2 exhibits a sharp drop, signaling a structural change in the overlayer. A continuous decrease of the reflected intensity is observed until 803 K, where the overlayer phase covers the entire surface. As mentioned previously, the changing electron reflectivity can be correlated to a change in atomic density of the overlayer phase. In this particular case, 796 K would mark the temperature where a substantial reduction of the Bi density in the overlayer phase sets in, and where the interatomic spacing between Bi atoms in the overlayer phase becomes large.

To understand this transition, we consider the changes in configurational entropy that occur in the narrow temperature interval between 796 and 803 K. The Helmholtz free energy F of the system is given by

$$F = A_{\sqrt{3}}\gamma_{\sqrt{3}} + (1 - A)\gamma_{\text{2D-gas}}, \tag{7}$$

where γ denotes the surface free energy of both phases, including configurational and vibrational entropy contributions. Because of the narrow temperature range in which the density changes of the overlayer occur, we only consider changes in configurational entropy of the two phases and assume the vibrational entropy difference to be constant. The configurational entropy of both phases depends on the relative Bi coverage. The relative coverage of the two phases is coupled through the area fraction A, as well as the total Bi coverage that is used during the experiment. Especially the latter makes

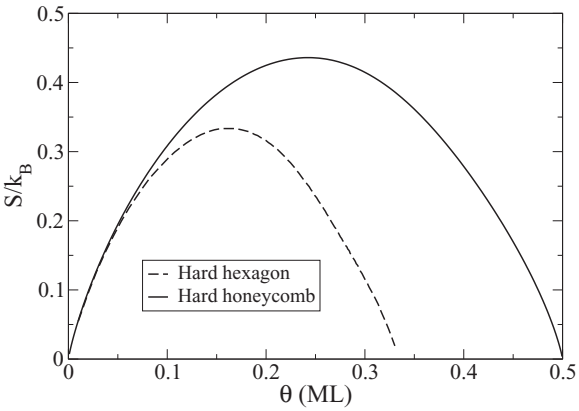

FIG. 7. Configurational entropy of the $\sqrt{3}$ phase as calculated using the hard-hexagon model, and that of the hard honeycomb model, calculated for the overlayer phase, following Refs. [26,27].

an exact quantitative description tedious, because the precise amount of Bi that resides in 3D Bi/Cu structures is not known. The hard-hexagon configurational entropy of the $\sqrt{3}$ phase can be directly calculated [25]. Given the structure of the overlayer phase [6,12], the configurational entropy of the overlayer phase can be modeled as that of monomers on a hard honeycomb lattice. For low coverages it approaches that of a simple lattice gas:

$$S = -k_b[(1 - \theta)\ln(1 - \theta) + \theta\ln(\theta)]. \tag{8}$$

It will deviate from this simple expression once the Bi atoms in the overlayer start to interact, but can be evaluated numerically [26]. The entropy for both the hard-hexagon and hard honeycomb models is plotted in Fig. 7. From the graph we see that the rapid change in density of the overlayer phase that starts at 796 K is not a coincidence. Between 796 and 803 K the configurational entropy of the $\sqrt{3}$ phase reduces strongly as a result of its rapidly decreasing Bi coverage, cf. Fig. 3. As a coverage of approximately 0.15 ML is reached for the $\sqrt{3}$ phase at 796 K, the reduction of the configurational entropy with decreasing Bi coverage becomes very significant. Any further decrease in coverage of the $\sqrt{3}$ phase would lead to an increase in the free energy of the system. Instead, the free energy can still be lowered by changing the area fraction A. This change in area fraction is accompanied by a change in density of the overlayer phase. The magnitude of this change in density that we estimate from the measured overlayer intensities of Fig. 2 is of the order of 25%–50%, but is hard to determine quantitatively because of the existence of 3D structures on the surface containing Bi. For these densities of the overlayer phase we start to move towards the top of the entropy curve of the hard honeycomb model in Fig. 7 and hence it would be energetically preferred to increase the area of the overlayer phase rather than further decrease the Bi coverage of the $\sqrt{3}$ phase. To evaluate the precise temperature where the transition occurs, we would have to find the complementary coverages of the overlayer and alloy phase where the slopes of the configurational entropy curves are equal, while also considering the formation energies of both phases. The entropy change associated with decreasing the coverage of the overlayer has to be equal to the entropy loss

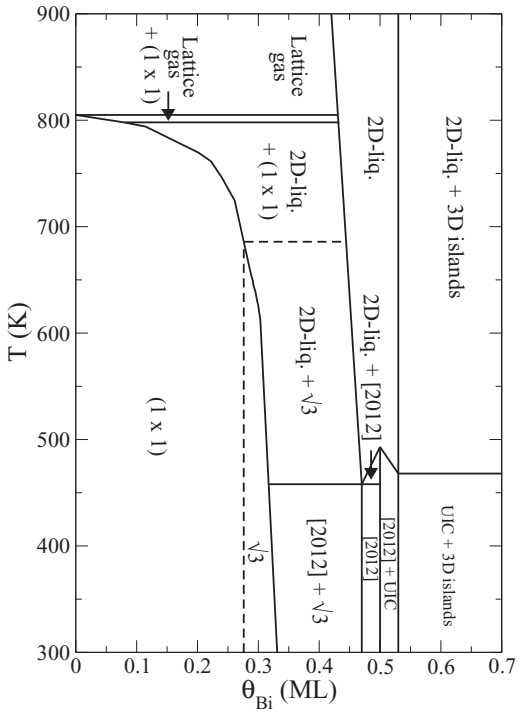

FIG. 8. The surface phase diagram of Bi/Cu{111}. We note that depending on the temperature and coverage trajectory that is used to reach a certain point in the phase diagram, a stable 3D Bi-Cu alloy phase can coexist with the depicted phases. The horizontal dashed line marks the temperature induced second-order order-disorder hard-hexagon phase transition that occurs in the $\sqrt{3}$ phase.

by decreasing the coverage of the alloy. One might speculate that the onset of this change in density of the overlayer alters the character of the overlayer from a 2D liquid to a 2D gas as a result, similar to the change from solid to liquid that is observed at lower temperatures [12]. A full and proper characterization of the nature of the overlayer, and, e.g., the latent heat that would be involved in the liquid to gas transition and the expansion of the 2D lattice gas with temperature, is however beyond the scope of the present work.

VI. CONCLUSIONS

In conclusion, we have investigated the structure of various Bi phases that form on Cu{111} using LEEM. A substitutional Cu{111}($\sqrt{3} \times \sqrt{3}$)R30°-Bi phase coexists with a Bi overlayer phase. The $\sqrt{3}$ alloy experiences a reduction in Bi coverage as a function of temperature. This leads to a gradual change in its elastic properties. Defect hardening by off-site Bi defects is observed for low densities of defects. At a critical Bi coverage of 0.276 ML an order-disorder transition occurs that dramatically modifies the elastic properties of the $\sqrt{3}$ alloy. It was found to completely dealloy at a temperature of 803 K. The behavior of the $\sqrt{3}$ phase is accurately described by the hard-hexagon model. The Bi overlayer phase was found to preserve its character of a 2D liquid up to a temperature of 796 K. Above that temperature the reduced configurational entropy of the $\sqrt{3}$ phase forces it to alter its density in such a way that the overlayer phase acquires more the character of a lattice gas of Bi adatoms rather than an overlayer. The Bi lattice gas eventually covers the entire surface area at 803 K.

Using the results that we have described in this paper, we have further refined the surface phase diagram for Bi on Cu{111} that we first published in Ref. [12], and replotted it in Fig. 8.

ACKNOWLEDGMENT

We thank Norm Bartelt for many useful and stimulating discussions.

[1] P. Gambardella, A. Dallmeyer, K. Maiti, M. C. Malagoli, W. Eberhard, K. Kern, and C. Carbone, Nature (London) **416**, 301 (2002).
[2] L. P. Nielsen, F. Besenbacher, I. Stensgaard, E. Laegsgaard, C. Engdahl, P. Stoltze, K. W. Jacobsen, and J. K. Nørskov, Phys. Rev. Lett. **71**, 754 (1993).
[3] Y. Tu and J. Tersoff, Phys. Rev. Lett. **98**, 096103 (2007).
[4] Edited by D. P. Woodruff, in *Surface Alloys and Alloy Surfaces* (Elsevier, Amsterdam, 2002), Vol. 10.
[5] D. P. Woodruff, Surf. Sci. **602**, 2963 (2008).
[6] D. Kaminski, P. Poodt, E. Aret, N. Radenovic, and E. Vlieg, Surf. Sci. **575**, 233 (2005).
[7] R. van Gastel, D. Kaminski, E. Vlieg, and B. Poelsema, Phys. Rev. Lett. **109**, 195501 (2012).
[8] R. van Gastel, D. Kaminski, E. Vlieg, and B. Poelsema, Surf. Sci. **603**, 3292 (2009).
[9] F. Delamare and G. E. Rhead, Surf. Sci. **35**, 172 (1973).
[10] F. Delamare and G. E. Rhead, Surf. Sci. **35**, 185 (1973).
[11] Y. Girard, C. Chacon, G. de Abreu, J. Lagoute, V. Repain, and S. Rousset, Surf. Sci. **617**, 118 (2013).
[12] D. Kaminski, P. Poodt, E. Aret, N. Radenovic, and E. Vlieg, Phys. Rev. Lett. **96**, 056102 (2006).
[13] E. Bauer, Rep. Prog. Phys. **57**, 895 (1994).
[14] J. de la Figuera, N. C. Bartelt, and K. F. McCarty, Surf. Sci. **600**, 4062 (2006).
[15] D. Schwarz, R. van Gastel, H. J. W. Zandvliet, and B. Poelsema, Phys. Rev. Lett. **109**, 016101 (2012).
[16] D. Schwarz, R. van Gastel, H. J. W. Zandvliet, and B. Poelsema, Phys. Rev. B **85**, 235419 (2012).
[17] K. H. Chae, H. C. Lu, and T. Gustafsson, Phys. Rev. B **54**, 14082 (1996).
[18] R. van Gastel, R. Plass, N. C. Bartelt, and G. L. Kellogg, Phys. Rev. Lett. **91**, 055503 (2003).
[19] J. M. Rickman and D. J. Srolovitz, Surf. Sci. **284**, 211 (1993).
[20] R. van Gastel, N. C. Bartelt, P. J. Feibelman, F. Léonard, and G. L. Kellogg, Phys. Rev. B **70**, 245413 (2004).

[21] G. W. C. Kaye and T. H. Laby, in *Tables of Physical and Chemical Constants* (Longman, London, 1993).
[22] M. J. Doyle, Polym. Eng. Sci. **40**, 330 (2000).
[23] R. J. Baxter, J. Phys. A: Math. Gen. **13**, L61 (1980).
[24] J. D. Eshelby, Acta Metall. **3**, 487 (1955).
[25] R. J. Baxter and S. K. Tsang, J. Phys. A: Math. Gen. **13**, 1023 (1980).
[26] L. D. Roelofs, T. L. Einstein, N. C. Bartelt, and J. D. Shore, Surf. Sci. **176**, 295 (1986).
[27] R. J. Baxter, Ann. Comb. **3**, 191 (1999).